Journal of Manufacturing Processes 134 (2025) 891–903

Contents lists available at ScienceDirect

Journal of Manufacturing Processes

journal homepage: www.elsevier.com/locate/manpro

Connecting texture development to die design in extruded flat products

Fabian Esterl [a,*], Maria Nienaber [b], Jan Bohlen [b], Noomane Ben Khalifa [a,b]

[a] Institute for Production Technology and Systems, Leuphana Universität Lüneburg, Lüneburg, Germany
[b] Institute of Material and Process Design, Helmholtz-Zentrum Hereon, Geesthacht, Germany

ARTICLE INFO

Keywords:
Die design
Texture development
Finite element analysis
Magnesium
Aluminum
Extrusion

ABSTRACT

This study investigates the local texture modification of two magnesium alloys (AZ31 and ZX10) and an aluminum alloy (AA6082) based on changes in the die design. For this purpose, a conventional flat die and a modified die, which has been additively manufactured to allow for a significant modification of the material flow, are investigated. Extrusion tests are carried out, followed by a comprehensive examination of the microstructure and local texture development. These experimental results are complemented by finite element analysis of the state variable distribution in the cross section of the extruded band. The results demonstrate that the texture change is connected to the strain path and can therefore be controlled based on the die design. This equally applies to all of the investigated alloys, despite their differences in crystallographic deformation and recrystallization behavior. Accordingly, a rotation of the dominant texture components about ND at the edge of the band of approximately 40°, 45°, and 20° is observed for AZ31, ZX10, and AA6082, respectively. These findings correlate well with the difference in rotation around ND between the dies of 39°, which is calculated numerically based on the deformation gradient tensor. Furthermore, AZ31 and ZX10 demonstrate a broadening of the basal planes in the TD when extruded with the modified die, which can be related to the increased shear strains in the ED/TD plane over the entire width of the band. For ZX10 specifically, a completely different texture is generated due to the combination of the broadened basal planes in TD, the rotation of the dominant texture component around ND, and its tilt in ED, characteristic of extruded Ca-containing Mg-alloys. The investigation on AA6082 further illustrates the importance of the effective temperature and strain rate in the forming zone for its texture development. While no significant change in the microstructure is evident, the increased heat dissipation and smoothed introduction of dislocations during extrusion with the modified die correlates with a transition from Cube to Goss as the dominant texture component.

1. Introduction

As the demand for improved energy efficiency and reduced emissions in the automotive and aerospace industries increases, the need for lightweight components meeting the required mechanical properties is becoming increasingly apparent [1,2]. Magnesium and aluminum alloys offer low density while maintaining sufficient strength properties and are therefore of growing interest for application as structural components [3,4]. Extrusion enables the production of profiles with continuous cross sections in a single step, reducing the production costs of such components significantly. However, the presence of high strains accompanied by unidirectional material flow during extrusion leads to the occurrence of distinct anisotropic mechanical properties [5,6]. These anisotropic properties are disadvantageous for further processing such as bending or deep drawing. To address the mechanical anisotropy, additional processing is required, consequently increasing the costs for these products.

Magnesium and aluminum significantly differ in deformation behavior and texture development during extrusion. Magnesium is characterized by a hexagonal close-packed (hcp) crystal structure. The activability of only three independent slip systems accounts for limited formability. Further, basal slip and extension twinning are dominant during forming, ultimately leading to a preferred orientation of the basal planes parallel to the stress direction or the forming of a predominant $\langle 10\bar{1}0 \rangle$ –prismatic fiber [7]. Additionally, its low stacking fault energy promotes dynamic recrystallization to dominate microstructure and texture development [8]. Here, increased process temperatures significantly favor grain growth. In contrast, aluminum features a face-centered cubic (fcc) crystal structure. Due to its high symmetry, twelve independent slip systems grant enhanced formability. Typical

* Corresponding author.
E-mail address: fabian.esterl@leuphana.de (F. Esterl).

https://doi.org/10.1016/j.jmapro.2024.12.078
Received 21 October 2024; Received in revised form 12 December 2024; Accepted 29 December 2024
Available online 11 January 2025

deformation textures after extrusion of aluminum consist of ⟨111⟩/⟨100⟩ −double fibers [9]. Furthermore, the high stacking fault energy promotes the dominant influence of dynamic recovery for microstructure and texture development [10]. Apart from these differences in deformation behavior and texture development, extruded magnesium and aluminum typically exhibit pronounced textures, generally associated with anisotropic mechanical properties [11].

Different strategies are described within the literature that target to influence microstructure and texture development in extrusion. For magnesium, one prominent approach is using rare earth (RE) or calcium as alloying elements [12]. The introduction of RE changes the texture and leads to the formation of a so-called “RE component” [13] which exhibits basal split peaks tilted towards the extrusion direction (ED) in the case of flat band extrudates [14]. Thereby, the mechanical properties of the extrudates can be modified. However, the addition of such RE is costly and may still result in anisotropic mechanical properties after extrusion based on non-symmetric distribution of grain orientations.

Alternatively, the die design can change the texture development within the extrusion process as changes in material flow also alter the strain state introduced into the material. In equal channel angular pressing (ECAP), the material is steered through a predetermined angle, which leads to advanced shear. Thereby, pronounced grain refinement and a modification of the texture occur. The integration of ECAP into extrusion illustrates that the type and strength of the textures of pure aluminum vary according to the deformation path [15]. The extrusion of AZ31 through ECAP confirms that the degree of grain refinement and the characteristics of the textures depend on the shear angle geometrically introduced by the die [16]. It is further stated that the anisotropy of the mechanical properties is significantly lower when compared to conventionally extruded profiles. Comparably, a turned-bearing extrusion die has been proposed [17]. Here, the channel of the bearing introduces additional shear strains as the material is displaced in the normal direction (ND), resulting in a change of texture, i.e. the alignment of basal planes received some tilting towards the ED. As a result, the tensile yield strength of the produced AZ31 band is increased compared to the conventionally extruded band. An alternative approach is to create an asymmetry on the choke angle or bearing length of the die, thereby introducing shear deformation in the ND [18,19]. The extrusion of AZ31 results in a weakening of the basal texture and a tilt towards the ED. This ultimately improves formability and reduces the planar anisotropy of the produced band. Similarly, die designs for transverse gradient extrusion have been proposed [20,21]. In this instance, the material flow exhibits displacement parallel to the transverse direction (TD). In the resulting AZ31 bands, the basal planes are also tilted towards the ED in an apparent change of the texture, and further texture components are produced in the TD, ultimately improving the formability of the band. Alternatively, a spiral die has been proposed to allow adjustment of the basal texture of AZ31 in extruded rods [22]. This design introduces circumferential shear deformation, which serves to suppress the activation of basal slip. In conjunction with the axial shear deformation, this leads to repeated transitions between basal and prismatic slip.

In the case of aluminum alloy extrusion, recent studies have focused on optimizing porthole die designs to achieve uniform metal flow and improved welding quality [23,24]. Nevertheless, it has been shown that modifications to the bridge geometry result in significant modification of the microstructure and texture development of extruded AA6082 bands [25]. The numerical investigation indicates that the strain, velocity, and temperature distribution in the cross section of the profiles differ when a flat bridge die is used as opposed to a streamlined bridge die. This leads to the formation of Cube, Goss, and $Cube_{RD}$ textures rather than Copper components near the weld line, consistent with increased recrystallization due to a higher local strain rate. Similarly, it has been demonstrated that alterations to the bridge geometry can markedly influence the mechanical properties of the resulting AA6063 profiles [26]. Equivalently, the incorporation of baffle-blocks into the die has been proposed to enhance the local strain amount and improve the uniformity in the cross section of the profile [27].

In summary, several studies have investigated the potential of the die design to alter the microstructure and texture development in extruded profiles. Consequently, alternative die designs have been proposed that facilitate the modification of the strain history experienced by the material during extrusion. While the majority of the studies employ finite element (FE) models to reveal the mechanisms responsible for the texture modification, the knowledge of beneficial state variables for specific texture control based on deformation remains scarce. It is noteworthy that none of the studies make use of additive manufacturing to significantly alter the geometry of the press channel with the intention of controlling the material flow and associated strains. However, selective laser melting enables additive manufacturing of extrusion dies with structures that would otherwise be unattainable, such as complex internal cooling channels [28], while achieving comparable mechanical properties that can withstand the high pressure and temperature of the extrusion process [29].

In a previous study, a new concept of extrusion dies based on additive manufacturing has been developed, which allows control over the material flow [30]. It has been demonstrated that material-dependent changes in the microstructure and thus the mechanical properties are achievable. The present study directly links the microstructure and texture development to the local state variables (strain, strain rate, temperature) generated by the die design. Due to the differences in crystallographic deformation and recrystallization behavior, two magnesium alloys, AZ31 and ZX10, and an aluminum alloy, AA6082, are experimentally investigated. An FE model is set up to identify the flow characteristics and state variables in the cross section of the extruded band and validated against experimental results.

2. Materials and methods

The study is divided into an experimental setup, including manufacturing of the extrusion billets, extrusion, characterization of the billets and the extruded bands, and a numerical setup, including the material modeling, setup of an FE model and the post-processing of the simulation results. The procedure of this study is summarized in Fig. 1.

2.1. Experimental setup

The magnesium alloys, AZ31 and ZX10, were manufactured using a modified gravity casting process with directional solidification within a crucible. A comprehensive description of this process can be found in [31]. Subsequently, the extrusion billets were machined to achieve a diameter of 49 mm and a length of 75 mm. Both magnesium alloys were subjected to a heat treatment at 400 °C for 16 h. These parameters were repeated from earlier work [12] to maintain homogeneity and solid solution of alloying elements in the alloys. In addition, the aluminum alloy AA6082 was maintained in the supplied extruded and T6511 temper condition for the present study and then turned into the required dimensions. The chemical compositions of the two magnesium alloys and the aluminum alloy are summarized in Tables 1 and 2.

Fig. 2 illustrates the initial microstructure of the extrusion billets. For AZ31 and ZX10, a representative microstructure is depicted in the as-cast condition, characterized by the presence of large globular grains. In contrast, AA6082 exhibits a fine-grained extruded microstructure, with grains aligned in the direction of deformation.

The extrusion experiments were conducted using a 2.5 MN automatic extrusion press (*Müller Engineering*, Sand/ Todtenweis, Germany). The direct extrusion tests were performed under constant conditions, with a consistent extrusion ratio of 1:33 and ram speed of 1 mm/s. Both magnesium alloys were extruded at an initial temperature of 350 °C, reflecting on the differences in recrystallization behavior between the alloys [32]. In the case of AA6082, the initial billet temperature was set at 450 °C in order to maintain the fine grain structure and high

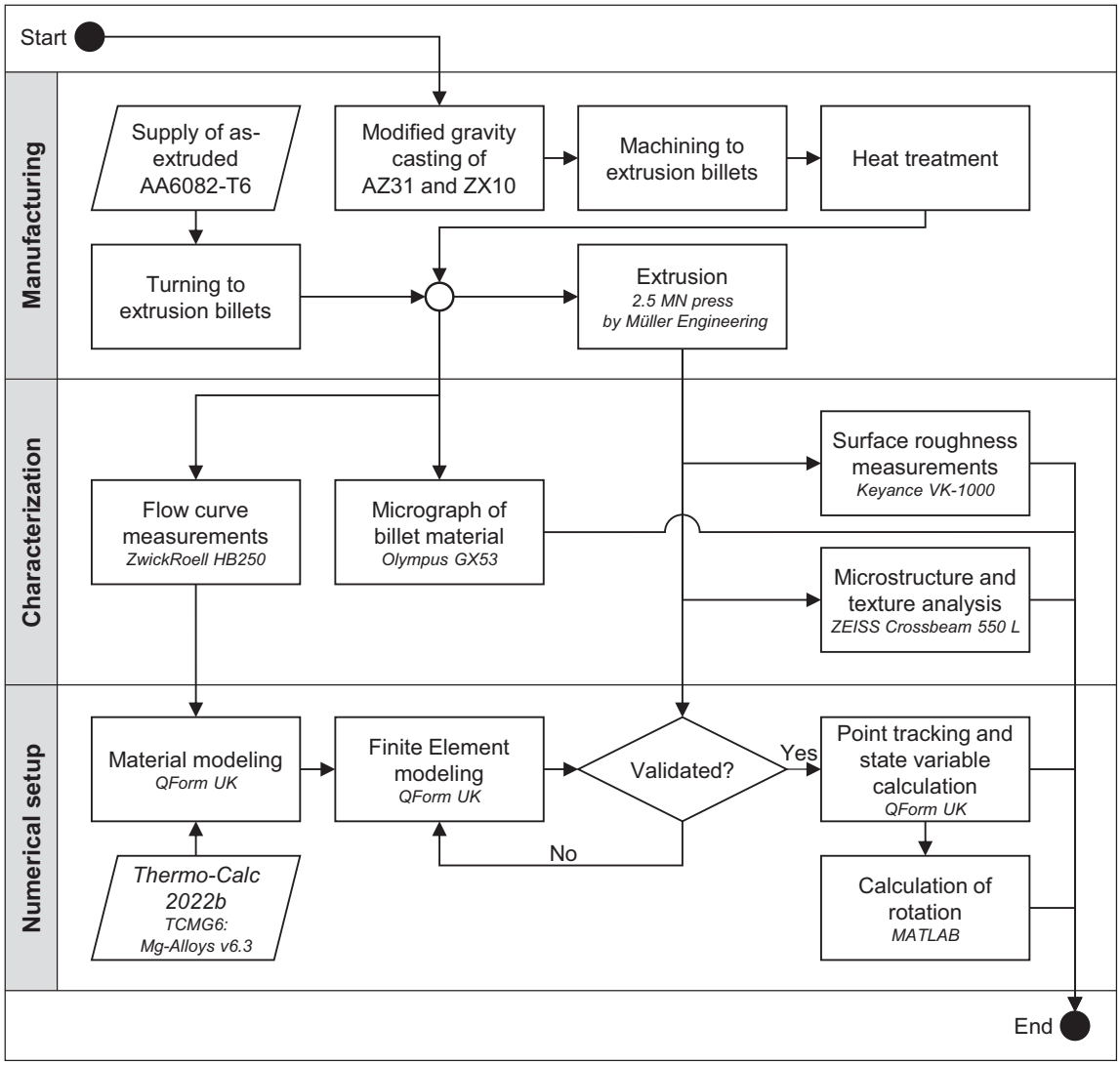

Fig. 1. Flow chart illustrating the procedure of the study, categorized into the phases of manufacturing, characterization, and numerical setup.

Table 1
Chemical composition of the investigated magnesium alloys (in wt.-%, Mg in balance).

Alloy	Al	Zn	Mn	Ca
AZ31	2.88	0.90	0.21	–
ZX10	–	1.01	–	0.14

Table 2
Chemical composition of the investigated aluminum alloy (in wt.-%, Al in balance).

Alloy	Si	Mn	Mg	Zn
AA6082	0.80	0.50	1.10	0.12

mechanical properties of the supplied extruded condition while respecting the typical extrusion temperature of the alloy. The billets were preheated for 30 min to the extrusion temperature. The extrusion involved the utilization of two different flat dies: a conventional flat die with an inlet angle of 90° (referred to as the conventional die) and a die with an additively manufactured inlet (referred to as modified die), described in detail in [30]. This modified die was produced by the *Fraunhofer Research Institution for Additive Manufacturing Technologies*. In this regard, selective laser melting (PBF-LB/M) was performed on a TruPrint 1000 (*TRUMPF*), employing a single laser beam with 200 W and a diameter of 55 µm. Subsequently, the inlet was solution heat treated and artificially aged in a vacuum to achieve a minimum hardness of 50 HRC, after which it was abrasive and shot blasted. However, no adjustment was made to the internal press channel. It is therefore evident that further attention must be paid to the surface quality of the extrudates.

The surface characterization of the extruded bands was performed using a confocal laser-scanning microscope VK-1000 (*Keyence*, Osaka, Japan). The surface roughness, as the mean arithmetic height S_a, was measured following the standard DIN EN ISO 25178-2.

A comprehensive examination of the texture along the sheet thickness (in ND) was conducted using a scanning electron microscope (*ZEISS* Crossbeam 550 L) with electron backscattered diffraction (EBSD). The analysis was performed with an accelerating voltage of 15 kV and a step size of 4 µm. The samples for the microstructure analyses were taken along the ED at the center of the band and measured with a step size of 0.6 µm. The preparation of the specimen followed established metallographic procedures, involving grinding and polishing. Additionally, an electropolishing step was carried out for 20 s at a voltage of 22 V, utilizing Struers AC2 solution maintained at a temperature of −20 °C.

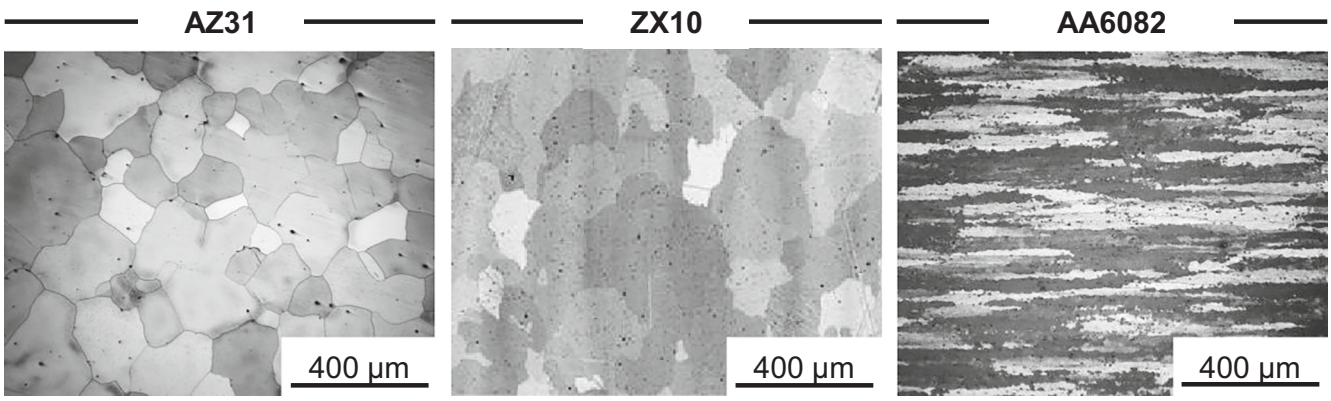

Fig. 2. Initial microstructure in the longitudinal direction of the extrusion billets of as-cast AZ31 and ZX10 and as-extruded AA6082.

2.2. Numerical setup

An FE model was set up using the simulation software *QForm UK*. Here, Lagrangian formulation is applied, and an explicit integration method is selected. A three-dimensional quarter model was constructed utilizing the General Forming module, acknowledging the distinct geometrical features of the dies in TD and ND. The imported conventional and modified die designs are shown in Fig. 3a and Fig. 3b, respectively.

To accurately reproduce the entire process, the assembly includes the billet, container, ram, and the investigated die. Here, the reference coordinate system is placed at the entrance of the die. Notably, the die and container were kept stationary, while the ram was subjected to a constant speed of 1 mm/s. To reduce the complexity of the simulation process, all tools are modeled as rigid bodies. The thermodynamic properties of the tool steel are sourced from the built-in material library in *QForm UK*. Accordingly, the heat transfer between the billet and the tools is considered.

In order to incorporate the elasto-viscoplastic behavior of the materials into the material models employed in *QForm UK*, a series of flow curves were achieved using a hydraulic universal testing setup (*Zwick-Roell* HB250) for compression tests within a temperature range of 250–450 °C and a strain rate range of 0.001–4 1/s. The remaining properties such as Young's modulus are taken from the built-in material library. As for the thermal conductivity and specific heat of the magnesium alloys, simulations were carried out using the software *Thermo-Calc 2022b* and the database TCMG6: Mg-Alloys v6.3.

The friction between the billet and the tools was incorporated by applying Levanov's friction law [33]:

$$\tau = m\left(\sigma_F \Big/ \sqrt{3}\right)\left(1 - exp(-1.25\,\sigma_N/\sigma_F)\right) \tag{1}$$

with τ as the friction stress, $m = 1$ as the friction factor, σ_F as the flow stress of the workpiece material and σ_N as the normal contact pressure.

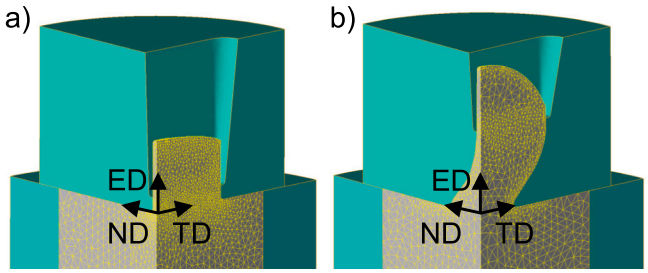

Fig. 3. Quarter model of a) the conventional and b) the modified die imported into *QForm UK* simulation software including the coordinate system and the workpiece mesh setup.

This model was chosen to prevent overestimating frictional stresses in case of low or high contact pressures.

All tools and the billet are discretized using three-dimensional tetrahedra as building blocks, with a minimum element edge length of 0.3 mm, a maximum element edge length of 2.0 mm, and an acceleration coefficient of 1.5. To correctly reproduce the contact of the billet with the press channel, the die's minimum and maximum element edge lengths are reduced using local adaptation to 0.1 mm and 0.5 mm, respectively. Based on steadily refined element edge length, this setup is considered adequate. To validate the numerical results, the ram load respective to the ram displacement is compared with the experimental results, see Fig. 4.

The numerical results demonstrate a high degree of correlation with the physical response of the system. The average relative error between numerical and experimental maximum ram load is 3 %. It should be noted that the experimental procedure requires the attachment of a puller after the beginning of material flow which results in a load drop and a new starting procedure which is not included in the simulation. However, it is observed that the simulation model systematically underestimates the ram displacement at which the maximum ram load is reached due to the rigid body assumption applied to the container and die.

To evaluate the flow characteristics and the resulting state variable distribution in the cross section of the band, *QForm UK*'s post-processing is used. To this end, three paths are created using point-tracking. Then, the strain tensor $\varepsilon \in \mathbb{R}^{3\times3}$, strain rate $\dot{\varepsilon}$, and temperature T are calculated for each path. To account for the local differences across the width (edge, quarter, and center) of the specimen, the final positions of the points are shifted along TD as represented in Fig. 5.

For the calculation of deformation-based rotation, four additional points are introduced around P1, P2, and P3. Three of these points are shifted by 0.1 mm along one of the principal axes, while the fourth is shifted by 0.1 mm along all axes. This methodology generates a cell representative of the area under investigation around P1-P3, with each cell consisting of a total of five points. Based on the initial position $A \in \mathbb{R}^{5\times3}$ and final position $B \in \mathbb{R}^{5\times3}$ of this cell, the affine transformation matrix F_{aff} is calculated for each time step. As F_{aff} also includes translation, it should be noted that $F_{\text{aff}} \in \mathbb{R}^{4\times3}$. Therefore, cartesian coordinates of initial position A are converted to homogeneous coordinates by appending a column of ones to A, thereby creating $A' \in \mathbb{R}^{5\times4}$. To obtain a unique F_{aff} based on A' and B, least squares is applied (see Eq. (2)).

$$A'\,F_{\text{aff}} = B \tag{2}$$

Transforming F_{aff} to a square matrix by removing the last row

$$F = \widetilde{I}\,F_{\text{aff}} \tag{3}$$

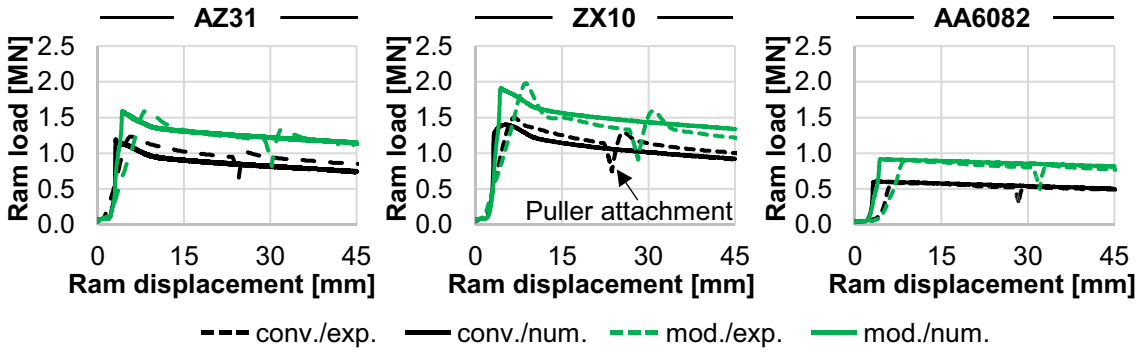

Fig. 4. Comparison of experimental (exp.) and numerical (num.) ram load-displacement curve for the conventional (conv.) and the modified (mod.) die.

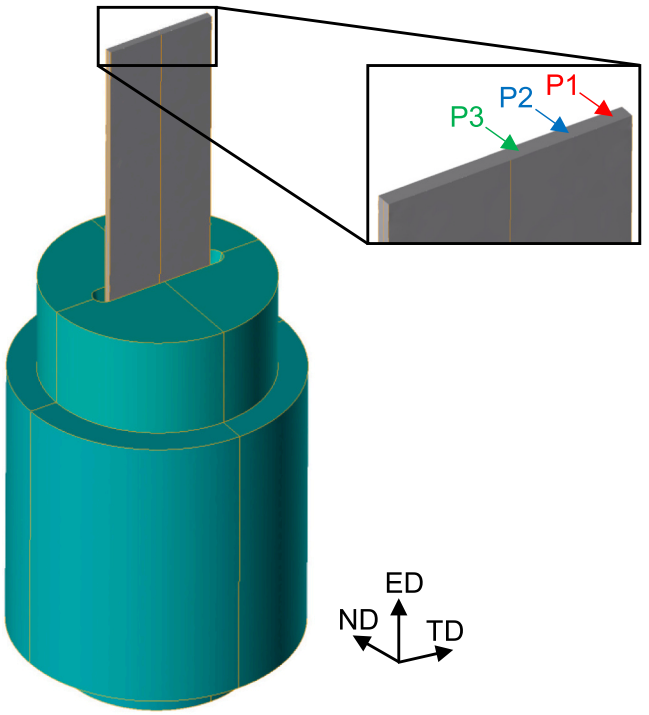

Fig. 5. Representation of the evaluation points P1 (edge), P2 (quarter), and P3 (center) in the TD/ND cross section for the numerical point tracking.

with $\widetilde{I} \in \mathbb{R}^{3\times4}$ as a truncated identity matrix, the deformation gradient tensor $F \in \mathbb{R}^{3\times3}$ is determined. F then only incorporates rotation and stretching.

$$F = R\,U \tag{4}$$

Using polar decomposition, the deformation gradient tensor is then split into unitary rotational matrix R and Hermitian stretch matrix U (see Eqs. (5) and (6)).

$$U = +\sqrt{F^T F} \tag{5}$$

$$R = F\,U^{-1} \tag{6}$$

The rotational matrix R incorporates the rotation around each axis TD, ND, and ED (see Eq. (7)).

$$R = R_{ED}(\Phi_{ED})\,R_{ND}(\Phi_{ND})\,R_{TD}(\Phi_{TD}) = \begin{pmatrix} R_{11} & \cdots & R_{13} \\ \vdots & \ddots & \vdots \\ R_{31} & \cdots & R_{33} \end{pmatrix} \tag{7}$$

Lastly, the angles of rotation Φ_{TD}, Φ_{ND}, and Φ_{ED} are obtained by Euler angle extraction from the rotational matrix R (see Eqs. (8)–(10)).

$$\Phi_{TD} = tan^{-1}(R_{32}/R_{33}) \tag{8}$$

$$\Phi_{ND} = tan^{-1}\left(-R_{31}\Big/\sqrt{{R_{32}}^2 + {R_{33}}^2}\right) \tag{9}$$

$$\Phi_{ED} = tan^{-1}(R_{21}/R_{11}) \tag{10}$$

3. Results

3.1. Surface quality

As a consequence of the additive manufacturing process employed in the production of the modified die, the surface of the modified die's press channel exhibits a markedly increased level of roughness. Following the extrusion tests, the press channel was cleaned and inspected. However, no evidence of wear was identified, consistent with existing work [29]. As for the surface quality of the extruded flat bands of the conventional die, only minor defects are observed, see Fig. 6a. Also, the surface topography shows a mostly homogeneous surface height over the width of the band, see Fig. 6b. However, when using the modified die, streaking defects are visible. Consistently, the surface topography shows abrupt changes in the measured surface height when moving in TD, most notably for ZX10. This is also reflected by the increased average surface height S_a of all bands extruded with the modified die, ranging from 7.9 µm – 12.9 µm as compared to 3.0 µm – 4.1 µm when using the conventional die.

3.2. Microstructure and texture development

Fig. 7 illustrates the microstructures in the ED/ND plane of the bands extruded with the conventional and the modified die, observed at the center of the band of each material. These are presented using inverse pole figure (IPF) maps with an orientation-dependent color code, alongside the characteristic average grain size (GS). While a color gradient within a grain displays a variation in crystallographic orientation and is therefore linked to deformed grains, a recrystallized grain shows no discernible difference in color.

The conventionally extruded AZ31 band exhibits a bimodal grain structure, comprising globular fully recrystallized grains and partially recrystallized grains straightened in ED. This is a typical result for an extruded band of this material [34]. In the band extruded with the modified die, these elongated grains are no longer present. Further, there is a slight increase in average grain size (13 µm and 15 µm).

The conventionally extruded ZX10 band exhibits a fully recrystallized globular microstructure. While also generating a fully recrystallized globular microstructure, extrusion with the modified die results in a markedly more pronounced grain growth (approximately doubling the average grain size from 16 µm to 28 µm), in comparison to the average

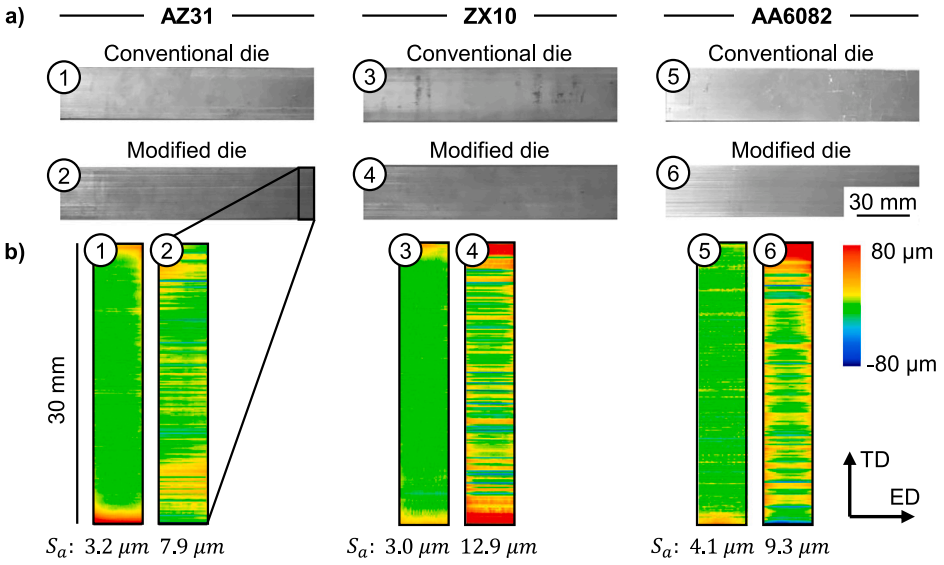

Fig. 6. Surface quality indicated by a) the macrograph of the surface of the extruded flat bands and b) the measured surface topography including the mean arithmetic height S_a.

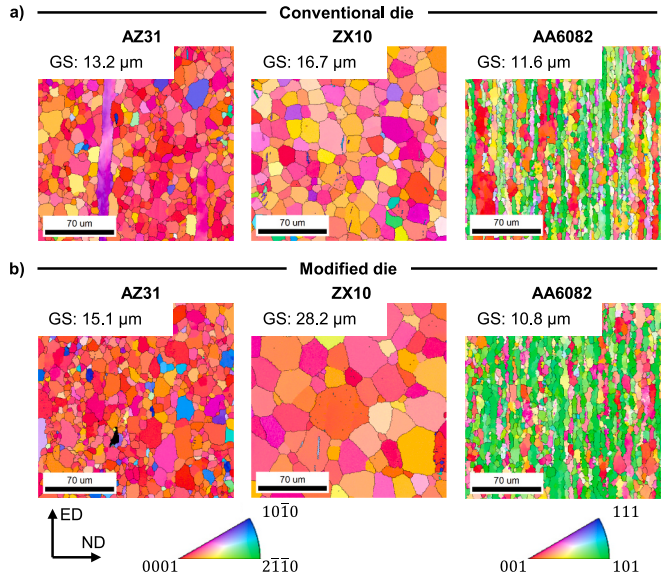

Fig. 7. Microstructure at the center of the extruded flat bands with the average grain size (GS) using inverse pole figure maps for a) the conventional and b) the modified die.

grain size of the conventionally extruded ZX10 band. It has been demonstrated in previous work [35] that the coarsening of the microstructure of this alloy is associated with a heightened thermal impact, which can be attributed to an increase in temperature or strain rate.

The microstructure of AA6082 exhibits notable differences compared to that of the two magnesium alloys. However, the use of the conventional and the modified die results in only slight deviations in the extruded microstructures. In both cases, the microstructure displays partial recrystallization with elongated grains in ED. Additionally, the average grain size is comparable in the two bands (~11 µm).

The texture, i.e. the crystallographic orientation distribution of the microstructure, was measured using EBSD across the band thickness at three locations surrounding the evaluation points (P1, P2, and P3), that are shown in Fig. 5. At each location, a measuring area of about 2.8 mm in TD and 1.4 mm in ND was defined. In the case of magnesium alloys, the (0001) pole figure is used to identify the orientation of the basal planes, while the (10−10) pole figure is employed to indicate the orientation of the prismatic planes. With regard to aluminum, the (111) pole figure is utilized to illustrate the orientation of the close-packed planes, whereas the (100) pole figure is used to indicate the orientation of the fcc main plane [36]. The orientation of the crystallographic structure in the extruded bands and the ideal texture components for the materials examined in this study are illustrated in Fig. 8.

For AZ31 extruded with the conventional die (Fig. 9a), the typical texture consists of a distinct alignment of basal planes in the form of a basal (0001) ⟨10−10⟩ component which also correlates with six weak peak maxima in the (10–10) pole figure [37], as shown in Fig. 8. Furthermore, there is a pronounced (0001) basal fiber parallel to ND. At the edge of the band (P1), this component appears with a slight split peak tilt of basal planes towards ED. Additionally, most pronounced at the edge of the band (P1), a weak prismatic fiber parallel to ED is visible [34]. The distribution of basal planes in TD decreases towards the center of the band (P3). Furthermore, a slightly weakened texture is observed at P1 when compared to P2 and P3. Overall, these textures stem from the activation of deformation mechanisms including dominant basal slip [38] as well as concurrent dynamic recrystallization which is known to not alter the deformation textures distinctly in this alloy. Details can be found in [34,39].

In the texture development for the AZ31 bands extruded using the modified die (Fig. 9b), a clear change can be seen. At the edge of the band (P1), there is a distinct tilt of the basal planes out of the sheet plane towards ED of around 20° and rotation about ND of approximately 40° of the {0001} component as well as the related fiber. For P2, this tilt of basal planes out of the sheet plane is not as pronounced (~10°), but the rotation of the basal component (around ND) is still clearly recognizable with around 20°. In the center of the band (P3), no visible splitting of the basal component compared to the results obtained from extrusion with the conventional die can be found. However, it shows a more pronounced broadening of basal planes to TD rather than to ED. It should be noted that the prismatic fiber is less developed for all these points compared to the extrudates of the conventional die. In terms of texture intensity, the band extruded with the modified die shows the highest intensity at the edge (P1), contrary to the location after extrusion with the conventional die.

For the conventionally extruded ZX10 (Fig. 10a), the above-mentioned (0001) ⟨11−20⟩ component is degenerated and tilted ~30° from ND to ± ED at all positions. This texture component is typical for Ca-containing Mg-alloys as a result of the underlying recrystallization

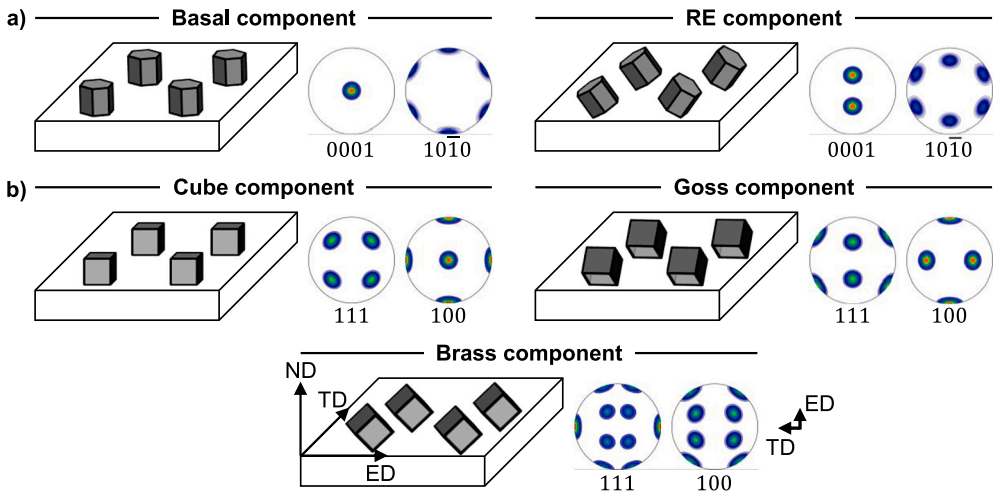

Fig. 8. Ideal crystallographic texture components observed in extruded bands of a) hexagonal and b) cubic materials.

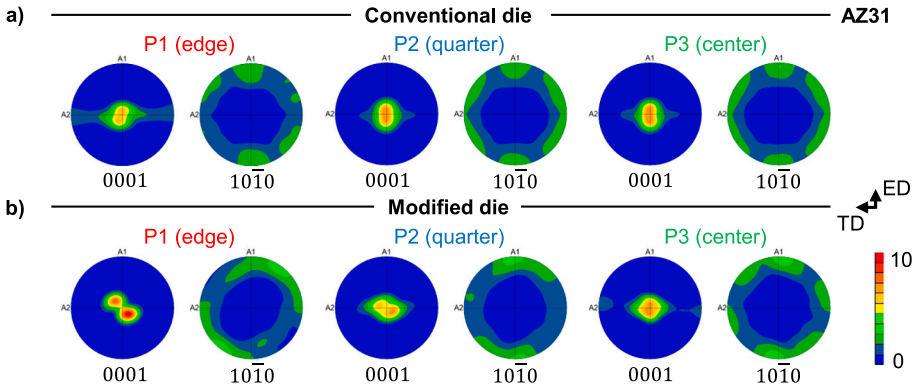

Fig. 9. (0001) and (10–10) pole figures at three different positions (edge, quarter, and center) in the ED/TD plane for AZ31 extruded with a) the conventional and b) the modified die.

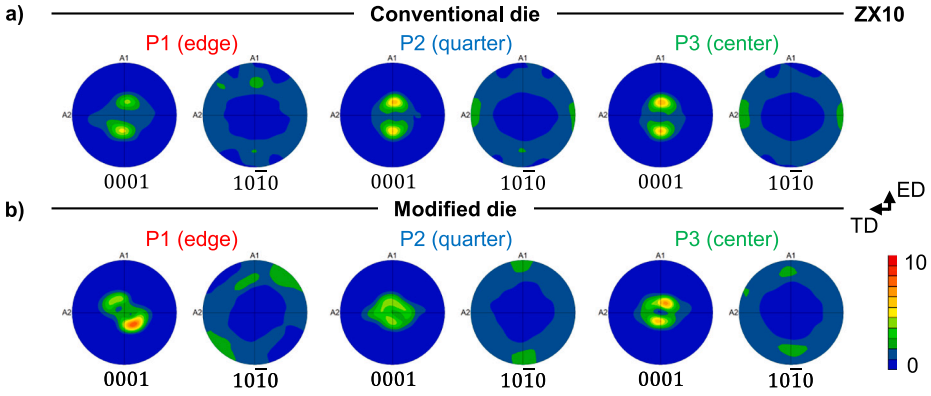

Fig. 10. (0001) and (10–10) pole figures at three different positions (edge, quarter, and center) in the ED/TD plane for ZX10 extruded with a) the conventional and b) the modified die.

behavior [12]. Furthermore, a weak fiber of the tilted basal component parallel to the ND is visible at all positions.

The bands extruded with the modified die (Fig. 10b) show the splitting of the basal planes out of the normal direction (tilting to ED). Comparing the tilt with results from the conventional die, the tilt angle varies according to the position. While P1 shows an increase in tilt of approximately 10°, P2 and P3 show a reduction of about 20°. The rotation around the ND is still clearly pronounced for ZX10 at around 45° for P1. For P2 and P3 the rotation of the basal component is less distinct. In contrast, these positions show a very clear broadening of the basal planes towards TD. This is more pronounced in P2 than in P3, ultimately leading to the weakest texture intensity. It is noticeable that P2 and P3 show characteristics described as a “donut” shape texture as fiber. In recent literature, this type of texture is associated with low mechanical anisotropy and enhanced formability [40].

To analyze the texture of the aluminum alloy (AA6082), the (111)

and (100) pole figures are shown in Fig. 11. Due to the multiplicity of aluminum textures, only the main components (with the highest intensities) are considered in the following, see Fig. 8.

For the extrudates of the conventional die, all positions show a dominant Cube component as texture. However, the presence of a Brass component is visible. These kinds of textures are typical for extruded AA6082 [41] and associated with the recrystallization of the material [42]. The variation of the textures as well as their strength is insignificant with respect to the three different positions.

The extrusion with the modified die leads to a major change in the texture. Now a Goss component dominates all positions. However, there is a variation in the orientation of the component depending on the analyzed position. As with AZ31 and ZX10, the rotation around ND seems to depend strongly on the position in the band. Again, P1 shows the strongest rotation around ND with approximately 20° from the original Goss position, while P3 shows no significant rotation around ND.

3.3. Flow characteristics

To investigate the influence of the altered channel on the material flow and the state variables in the TD/ND cross section, the three paths (P1-P3) are evaluated using point-tracking. In Fig. 12, the material flow lines in the ED/TD and ED/ND cross sections are shown. The position of the die exit for the conventional die is located at 2 mm as the coordinate in ED, whereas the press channel of the modified die ranges up to 14 mm in ED.

The simulation results for the conventional die demonstrate that the flow lines are largely consistent across all paths in both the ED/TD and ED/ND cross sections (Fig. 12a). Upon entering the die, the flow paths become parallel, indicating no further change in the flow direction. In the case of the modified die (Fig. 12b), the flow lines demonstrate more pronounced bending near the entrance reflecting the increased initial compression in the TD relative to the conventional die. Furthermore, upon entering the modified die, there is a noticeable change in the material flow as the modified die directs the material in the TD.

In Fig. 13, the strain paths experienced by the material as it passes through the conventional and the modified die are shown. In general, significant strains in ED and compression in the TD and ND throughout the entire cross section of the band extruded with the conventional die are calculated (Fig. 13a). However, the compression in TD is more pronounced near the edge of the band (P1), following the bending of the flow line just before entry of the die. In the case of the modified die, significantly reduced strains in ED, especially at the edge of the band, are calculated (Fig. 13b). Here, positive strains in TD are introduced, due to the displacement in TD. However, the compression in ND remains comparable with that of the conventionally extruded band for all paths.

Similarly, the shear strain paths experienced by the material as it passes through the conventional and the modified die are shown in Fig. 14. While no significant shear strain in TD/ND is calculated, significant shear strains in ND/ED plane occur throughout the entire cross section of the band when the conventional die is used (Fig. 14a). It is noteworthy, that the shear strain in ED/TD is less pronounced in the center of the band (P3), while minor negative shear strain in ED/TD is observed at the edge of the band. The application of the modified die results in a notable increase in shear strains in TD/ND and ED/TD, particularly at the edge of the band (Fig. 14b). Furthermore, the shear strain in ND/ED is also significantly reduced, while in the center it remains comparable to that of the conventionally extruded band. A detailed comparison of the final strain states for each respective point and both die designs is presented in Table 3. Here, the difference between the two dies in the final strain state $\Delta\varepsilon$ is also provided.

In Fig. 15, the results of calculated rotational angles Φ around each axis for all of the paths are shown. The final rotation states and the difference $\Delta\Phi$ between the two die designs are summarized in Table 4. In agreement with the results of the shear strains, the absolute rotation around each axis is highest at the edge (P1) and decreases towards the center of the band for both dies. However, comparing the rotational values between the dies, the absolute rotation around ND is significantly higher for the modified die at all positions. The increase in rotation is most pronounced at the edge of the band, thereby increasing the in-plane rotation gradient around ND. Regarding P2 and P3, the rotation around TD is decreased, ultimately steepening the difference in rotation in the cross section of the band extruded with the modified die. In contrast, only slight changes to the final rotation states are generated concerning the rotation around ED.

The changes in the material flow also lead to deviations in the strain rate when passing through the die, as shown in Fig. 16. For the conventional die, the maximum strain rate is reached at the die entrance, where the material is compressed to the final geometry. Here, the strain rate is homogenous and reaches a maximum of approximately 12 s^{-1}. The deformation ceases once the material passes the entrance, causing the strain rate to decline rapidly.

In contrast, the modified die design reaches its maximum strain rate at the die exit, coinciding with the attainment of the final geometry. At the periphery (P1), the maximum is about 8 s^{-1}, while at the center (P3), it reaches only about 4 s^{-1}. Notably, due to the continuous change of shape, the strain rate remains elevated throughout the entire die length.

Regarding the temperature development, there are only minor differences in the cross section of the bands. However, as the deformation leads to heat generation in the forming zone, the temperature development of the conventional and modified die differ significantly. Further, as the investigated alloys show distinct thermal behavior, noticeable differences for the varying alloys are found. However, the temperature development across all alloys follows a similar pattern, as shown in Fig. 17. Upon entering the die, the temperature remains close

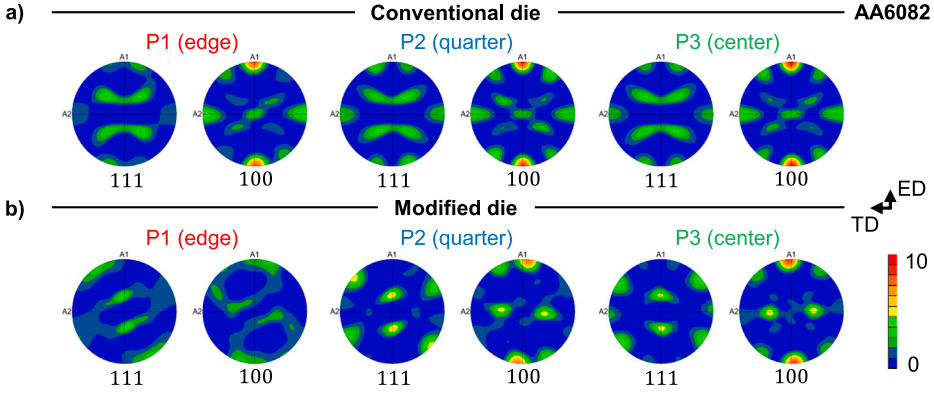

Fig. 11. (111) and (100) pole figures at three different positions (edge, quarter, and center) in the ED/TD plane for AA6082 extruded with a) the conventional and b) the modified die.

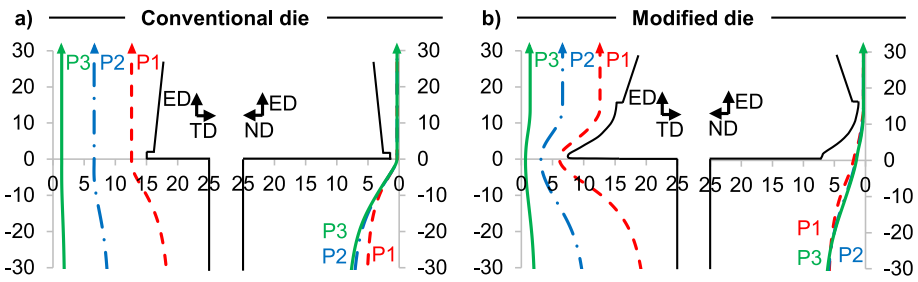

Fig. 12. Material flow lines in the ED/TD and ED/ND cross sections of P1-P3 while passing through a) the conventional and b) the modified die.

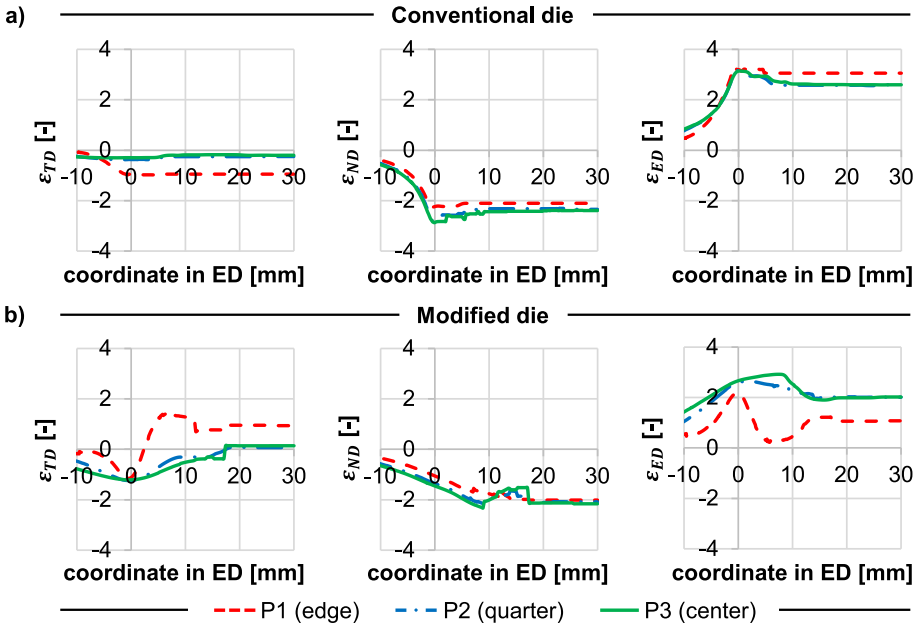

Fig. 13. Strain paths of P1-P3 while passing through a) the conventional and b) the modified die.

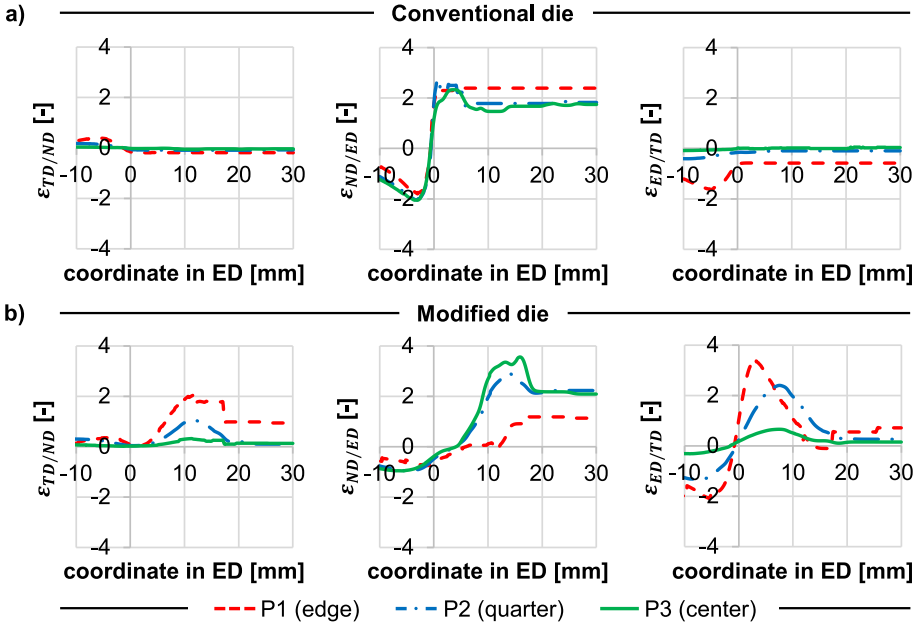

Fig. 14. Shear strain paths of P1-P3 while passing through for a) the conventional and b) the modified die.

Table 3
Comparison of the final strain states introduced by the conventional (conv.) and the modified (mod.) die.

	ε_{TD} [−]			ε_{ND} [−]			ε_{ED} [−]			$\varepsilon_{TD/ND}$ [−]			$\varepsilon_{ND/ED}$ [−]			$\varepsilon_{ED/TD}$ [−]		
	conv.	mod.	$\Delta\varepsilon_{TD}$	conv.	mod.	$\Delta\varepsilon_{ND}$	conv.	mod.	$\Delta\varepsilon_{ED}$	conv.	mod.	$\Delta\varepsilon_{TD/ND}$	conv.	mod.	$\Delta\varepsilon_{ND/ED}$	conv.	mod.	$\Delta\varepsilon_{ED/TD}$
P1	−0.9	0.9	1.8	−2.1	−2.0	0.1	3.0	1.1	−1.9	−0.2	0.9	1.1	2.4	1.1	−1.3	−0.6	0.7	1.3
P2	−0.3	0.1	0.4	−2.3	−2.1	0.2	2.6	2.0	−0.6	−0.1	0.1	0.2	1.8	2.2	0.4	−0.1	0.3	0.4
P3	−0.2	0.1	0.3	−2.4	−2.2	0.2	2.6	2.0	−0.6	0.0	0.1	0.1	1.7	2.1	0.4	0.0	0.2	0.2

to the initial value (350 °C for AZ31 and ZX10, and 450 °C for AA6082). Within the die, the deformation increases the temperature to a maximum, steadily decreasing as the material exits the die. In the case of the conventional die, the temperature peaks at 421 °C for AZ31, 428 °C for ZX10, and 483 °C for AA6082 (Fig. 17a). Consequently, the absolute temperature increase due to deformation is 71 °C for AZ31, 78 °C for ZX10, and 33 °C for AA6082.

Due to higher deformation in the modified die, a considerably higher temperature development in the forming zone is calculated (Fig. 17b). The temperatures of the magnesium alloys increase from 350 °C initial temperature up to 475 °C for AZ31 and 492 °C for ZX10. Here, for AA6082, the temperature increases to about 521 °C from initially 450 °C. Therefore, the modified die leads to heat generation in the forming zone significantly higher than that of the conventional die, with increases of 125 °C for AZ31, 142 °C for ZX10, and 71 °C for AA6082.

4. Discussion

The numerical results highlight significant changes in the flow characteristics and the associated state variables, especially in the forming zone. Here, noticeable changes to the strain states, the strain rate, and the temperature development are emphasized, granting discussion of changes in microstructure and texture development. Furthermore, the local differences in state variables are also reflected in the texture developed in the extruded bands, thereby enabling the connection of locally generated textures and state variables.

In terms of microstructure evolution, both magnesium alloys show grain coarsening, which is only slight for AZ31 and more pronounced for ZX10 when extruded with the modified die. As the modified die leads to a smooth introduction of dislocations and increased temperatures in the forming zone (see Fig. 16 and Fig. 17), grain growth especially for ZX10 is plausible due to a higher thermal impact in terms of the recrystallization kinetics for the modified die, see Fig. 17. Unlike AZ31, ZX10 alloy also exhibits a pronounced tendency for grain growth due to a distinct difference in the recrystallization mechanisms. Related work [12] has investigated this difference, including an alloy-specific alteration in the character of the dynamic recrystallization mechanism. Instead of a dominant mechanism of grain nucleation and growth, a continuous mode of recrystallization by rearrangement and rotation of low-angle grain boundaries towards high-angle boundaries has been proposed [43]. For AA6082, no visible change in the resulting grain structure is achieved. The change of effective temperature in the forming zone from about 483 °C for the conventional die to 521 °C when extruded with the modified die on the microstructure development of AA6082 is therefore only marginal.

As the local textures differ, the connection towards the state variables at the corresponding location is sensible. At the periphery (P1) of the conventionally extruded AZ31 band, a distinct split peak and a slight tilt of the basal planes towards ED are observed. This is accompanied by a weak prismatic fiber aligned with ED. A similar texture is documented by Yang et al. [18], who state, that due to the increase of shear, the basal planes tilt towards the imposed shear direction. The numerical analysis supports this statement, as higher shear strains in ED/TD can be found close to the dead metal zone, decreasing towards the center.

As for the modified die, the texture of AZ31 is significantly altered, distinctively tilting the basal planes out of the sheet plane to ED and rotating the {0001} component as well as the related fiber around ND. This is most dominant at the edge of the band (20° and 40° around ED and ND, respectively) while less tilt and rotation can be found at P2 (10° and 20°, respectively), and no visible change in tilt or rotation is found at the center. Xu et al. [44] describes a comparable texture modification in AZ31 sheets. They report that the velocity along TD and the velocity gradient along ED cause the gradient of texture rotation around ND present in the cross section. In agreement, the numerical analysis of the modified die design highlights the introduction of positive strains in TD (corresponding to the velocity component in TD) and significantly

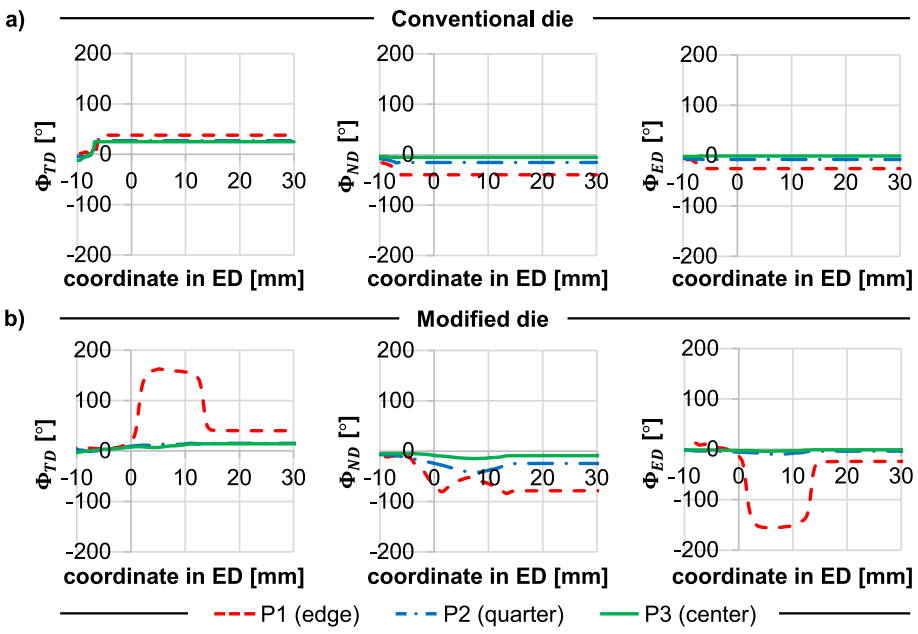

Fig. 15. Rotation of P1-P3 while passing through a) the conventional and b) the modified die.

Table 4
Comparison of the rotational angles of paths P1 (edge), P2 (quarter), and P3 (center) introduced by the conventional (conv.) and modified (mod.) die.

	Φ_{TD} [°]			Φ_{ND} [°]			Φ_{ED} [°]		
	conv.	mod.	$\Delta\Phi_{TD}$	conv.	mod.	$\Delta\Phi_{ND}$	conv.	mod.	$\Delta\Phi_{ED}$
P1	38	40	2	−40	−79	−39	−26	−24	2
P2	27	15	−12	−15	−24	−9	−8	−4	4
P3	25	14	−11	−5	−9	−4	−1	−1	0

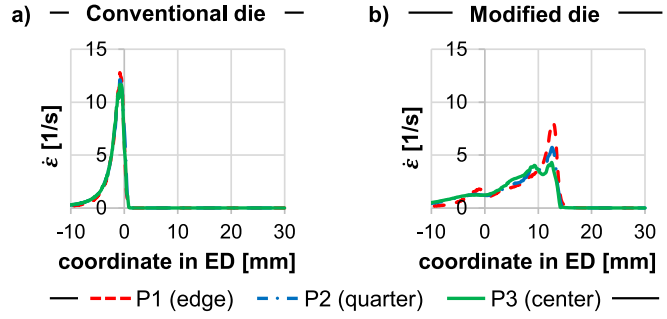

Fig. 16. Strain rate of P1-P3 while passing through a) the conventional and b) the modified die.

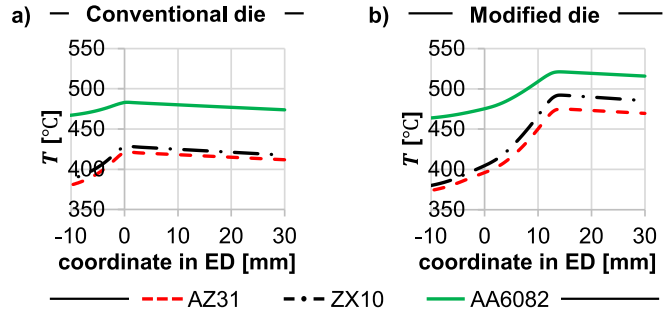

Fig. 17. Temperature development of AZ31, ZX10, and AA6082 while passing through a) the conventional and b) the modified die.

reduced strains in ED at the edge of the band. However, the rotation of the dominant texture component around ND can also be interpreted using the numerically calculated rotation based on the deformation gradient tensor. When comparing the rotation of conventional and modified die, the difference is in good agreement with the experimentally observed rotation of dominant texture components. Therefore, at the edge of the band, about 39° of difference in rotation around ND is calculated while in the center, the difference is only about 4°. Lastly, the presence of broadened basal planes even in the center can be related to the increased shear strains in ED/TD plane when extruded with the modified die, akin to the conventionally extruded band at the edge.

When extruded with the conventional die, ZX10 obtains a degenerated and tilted texture component throughout the whole width of the band. This texture is typical for Ca or RE-containing Mg—Zn alloys and is known as “RE-texture” [12]. The addition of Ca changes the dynamic recrystallization, randomizing the crystallographic orientation of the components as described in [45].

Using the modified die, the split texture component of ZX10 is not only tilted in ED like with the conventional die but the basal component is rotated around ND at about 45° near the edge of the band, which corresponds well with the rotation found in AZ31 and numerically assessed rotation based on deformation gradient tensor. Consistently, at P2 and P3, this rotation around ND is not as pronounced. However, the basal planes broaden towards TD, thereby generating a completely different texture as fiber. Victoria-Hernández et al. [40] report, that these textures can be associated with enhanced formability and reduced mechanical anisotropy. Thereby, the importance of increased shear strains in ED/TD as well as slight rotation about ND and tilt about TD for beneficial texture modification of ZX10 is highlighted.

For AA6082, the texture obtained with the conventional die is consistent with the existing literature as a dominant Cube component

results. However, extrusion with the modified die shifts the dominant texture component from Cube to Goss in the whole width of the band. This type of texture transformation for aluminum from Cube to Goss component has also been documented by Chen et al. [46], who emphasize that the presence of Goss is attributed to the recrystallization. Wang et al. [26] demonstrate a comparable transition from Cube to Goss, related to a die geometry that introduces reduced strain rates. In agreement, the numerical analysis shows reduced strain rates at all positions, see Fig. 16. Further, an increased heat generation in the modified die is calculated, raising the effective forming temperature of AA6082 to 521 °C, compared to 483 °C when extruded with the conventional die as shown in Fig. 17. Due to the shift in dominant texture component over the entire width of the band, it is hypothesized that predominantly the decrease in strain rate and increase in temperature facilitates the texture shift from a Cube to a Goss component although no visible impact on the underlying grain structure is obtained, see Fig. 7. Therefore, control over the strain rate and the effective temperature in the forming zone for specific texture formation and orientation is integral. As for the die design, the strain rate can be influenced by changing the magnitude of deformation introduced over the length of the die. Furthermore, the effective deformation temperature can separately be altered based on changes in the initial billet and tool temperatures. Nevertheless, the dominant texture components are yet again locally rotated. At the edge of the band (P1), a rotation of the Goss component of about 20° is identified when compared to the conventional orientation of the Goss component. This rotation decreases towards the center of the band, following the previous results of the magnesium alloys, and the numerically calculated rotation around ND.

5. Conclusions

As mechanical properties are known to be texture-dependent, the plastic anisotropy of extrudates is linked to texture development. In this study, the connection between changed state variables in the forming zone dictated by the die design and the subsequent microstructure and texture development is examined. Therefore, direct extrusion of flat bands has been carried out on AZ31, ZX10, and AA6082. The numerical data on strain states and rotation allows for the description of local changes in the crystallographic orientation, thus enabling the derivation of favorable state variables for each specific alloy characteristic. The key findings of the study can be summarized as follows:

1. The texture change is connected to the strain path and can therefore be controlled based on the die design. This applies equally to AA6082, an alloy that tends to demonstrate a recovery-dominated texture evolution; AZ31, an Mg alloy whose texture evolution due to recrystallization differs only slightly from the forming texture; and ZX10, an alloy whose recrystallization texture is distinctly altered compared to the pure forming texture.
2. All alloys under investigation show a rotation around the ND of the dominant texture components, which is most pronounced at the edge of the band (40°, 45°, and 20° for AZ31, ZX10, and AA6082, respectively) and decreasing towards the center where no significant rotation can be detected. These findings correlate well with the difference in rotation around ND between the dies of 39°, which is numerically calculated based on the deformation gradient tensor.
3. AZ31 and ZX10 show a slight broadening of basal planes in TD even in the center of the band when extruded with the modified die. These changes can be attributed to the increased shear strains in ED/TD generated by the modified die. For ZX10 specifically, due to the combination of these broadened basal planes in TD, rotation around ND, and the tilt in ED, characteristic of extruded Ca-containing Mg-alloys, a completely different texture is generated.
4. The investigation on AA6082 illustrates the significance of the strain rate and the effective temperature in the forming zone for its texture development. The modified die results in higher deformation, which in turn causes a significantly increased heat dissipation when compared to the conventional die while simultaneously reducing the strain rates. Accordingly, the dominant texture component is observed to transition from Cube to Goss. It is therefore evident that alterations to the die design and the processing conditions enable control over the dominant texture component in AA6082 while, separately, a mechanically caused rotation of the texture component about ND remains achievable by changing the material flow.
5. As a consequence of additive manufacturing, the surface topography of the extruded bands demonstrates abrupt changes in the surface height along the TD, resulting in visible streaking defects. It is therefore necessary to undertake additional post-processing of the surfaces of the press channel of the additively manufactured die.

Overall, this study underscores the potential of texture modification in materials based on the die design, as deformation-based texture change has been demonstrated for materials with different crystallographic deformation and recrystallization behavior. Therefore, reverse engineering approaches can be used to identify die designs beneficial for distinct texture formation in specific alloys, ultimately enabling control over the mechanical properties and their directionality. In this regard, the potential of additive manufacturing for the realization of these new die concepts is highlighted. Future research will explore a broader range of such complex die designs and processing conditions, to enhance the comprehension of how state variables facilitate particular texture modification and, ultimately, the reduction of mechanical anisotropy. Furthermore, additional research is required to determine the optimal post-processing techniques for additively manufactured extrusion dies, intending to achieve an enhanced surface quality of the press channel.

CRediT authorship contribution statement

Fabian Esterl: Writing – original draft, Visualization, Validation, Methodology, Investigation, Formal analysis. **Maria Nienaber:** Writing – original draft, Visualization, Validation, Methodology, Investigation, Formal analysis. **Jan Bohlen:** Writing – review & editing, Supervision, Funding acquisition, Formal analysis. **Noomane Ben Khalifa:** Writing – review & editing, Supervision, Resources, Funding acquisition.

Declaration of competing interest

The authors declare that they have no known competing financial interests or personal relationships that could have appeared to influence the work reported in this paper.

Acknowledgments

The research has been funded by the Deutsche Forschungsgemeinschaft (DFG, German Research Foundation) under the project number: 455039650. The authors thank Dr. Björn Wiese for his help in supplying the thermodynamic material coefficients for the magnesium alloys, Amal Dallel for her contributions to the experiments and characterization, and Dr. Philipp Kohlwes for providing processing information on the additive manufacturing of the modified extrusion die inlet.

References

[1] Kulekci MK. Magnesium and its alloys applications in automotive industry. Int J Adv Manuf Technol 2008;39:851–65. https://doi.org/10.1007/s00170-007-1279-2.
[2] Dursun T, Soutis C. Recent developments in advanced aircraft aluminium alloys. Materials & Design (1980–2015) 2014;56:862–71. https://doi.org/10.1016/j.matdes.2013.12.002.
[3] Mordike B, Ebert T. Magnesium. Mater Sci Eng A 2001;302:37–45. https://doi.org/10.1016/S0921-5093(00)01351-4.
[4] Hirsch J. Aluminium in innovative light-weight car design. Mater Trans 2011;52:818–24. https://doi.org/10.2320/matertrans.L-MZ201132.

[5] Hill R. A theory of the yielding and plastic flow of anisotropic metals. Proceedings of the Royal Society of London Series A 1948;193:281–97. https://doi.org/10.1098/rspa.1948.0045.
[6] Kleiner S, Uggowitzer P. Mechanical anisotropy of extruded Mg–6% Al–1% Zn alloy. Mater Sci Eng A 2004;379:258–63. https://doi.org/10.1016/j.msea.2004.02.020.
[7] Pekguleryuz MO. Current developments in wrought magnesium alloys. In: Bettles C, Barnett M, editors. Advances in wrought magnesium alloys, fundamentals of processing, properties and applications. Cambridge: Woodhead Publ; 2012. p. 3–62. https://doi.org/10.1533/9780857093844.1.3.
[8] Myshlyaev M, McQueen H, Mwembela A, Konopleva E. Twinning, dynamic recovery and recrystallization in hot worked Mg–Al–Zn alloy. Mater Sci Eng A 2002;337:121–33. https://doi.org/10.1016/S0921-5093(02)00007-2.
[9] Hirsch J. Texture and anisotropy in industrial applications of aluminium alloys. Archives of Metallurgy and Materials 2005:21–34.
[10] Raabe D. 23 - recovery and recrystallization: Phenomena, physics, models, simulation. In: Laughlin DE, Hono K, editors. Physical metallurgy. Burlington: Elsevier Science; 2014. p. 2291–397. https://doi.org/10.1016/B978-0-444-53770-6.00023-X.
[11] Hirsch J, Al-Samman T. Superior light metals by texture engineering: optimized aluminum and magnesium alloys for automotive applications. Acta Mater 2013;61:818–43. https://doi.org/10.1016/j.actamat.2012.10.044.
[12] Nienaber M, Kainer KU, Letzig D, Bohlen J. Processing effects on the formability of extruded flat products of magnesium alloys. Front Mater 2019;6:459049. https://doi.org/10.3389/fmats.2019.00253.
[13] Stanford N, Barnett MR. The origin of "rare earth" texture development in extruded Mg-based alloys and its effect on tensile ductility. Mater Sci Eng A 2008;496:399–408. https://doi.org/10.1016/j.msea.2008.05.045.
[14] Nienaber M, Bohlen J, Yi S, Kurz G, Kainer KU, Letzig D. Influence of Ca addition on the dynamic and static recrystallization behavior of direct extruded flat profiles of Mg-Y-Zn alloy. Journal of Magnesium and Alloys 2023;11:3736–48. https://doi.org/10.1016/j.jma.2023.09.017.
[15] Suwas S, Arruffat Massion R, Tóth LS, Fundenberger J-J, Beausir B. Evolution of texture during equal channel angular extrusion of commercially pure aluminum: experiments and simulations. Mater Sci Eng A 2009;520:134–46. https://doi.org/10.1016/j.msea.2009.05.028.
[16] Jaehnke M, Gensch F, Mueller S. Modification of the anisotropy and strength differential effect of extruded AZ31 by extrusion-shear, proceedings of the 21st international ESAFORM conference on material forming: ESAFORM 2018, Palermo, Italy. 2018. p. 1–6.
[17] Liu L, Wei L, Xiao J, Bai S, Jiang B, He C, et al. Improving mechanical properties of AZ31 alloy sheets via novel turned-bearing extrusion by introducing shear strain. J Mater Res Technol 2023;24:9915–27. https://doi.org/10.1016/j.jmrt.2023.05.128.
[18] Yang Q, Jiang B, Tian Y, Liu W, Pan F. A tilted weak texture processed by an asymmetric extrusion for magnesium alloy sheets. Mater Lett 2013;100:29–31. https://doi.org/10.1016/j.matlet.2013.02.118.
[19] Yang Q, Jiang B, He J, Song B, Liu W, Dong H, et al. Tailoring texture and refining grain of magnesium alloy by differential speed extrusion process. Mater Sci Eng A 2014;612:187–91. https://doi.org/10.1016/j.msea.2014.06.045.
[20] Xu J, Jiang B, Kang Y, Zhao J, Zhang W, Zheng K, et al. Tailoring microstructure and texture of Mg–3Al–1Zn alloy sheets through curve extrusion process for achieving low planar anisotropy. Journal of Materials Science & Technology 2022;113:48–60. https://doi.org/10.1016/j.jmst.2021.09.023.
[21] Xu J, Zhao J, Jiang B, Chen X, Yang Q, Zhou N, et al. Effect of transverse gradient extrusion process on texture and mechanical properties of Mg–3Al–1Zn alloy sheets. J Mater Res Technol 2023;27:6171–81. https://doi.org/10.1016/j.jmrt.2023.11.090.
[22] Wu W, Chen W, Wang X, Wang W, Zhang W, Liu X, et al. Texture adjustment approach of magnesium alloys via variable strain path calculated by an integrated finite element-viscoplastic self-consistent model. Journal of Materials Science & Technology 2024;184:15–31. https://doi.org/10.1016/j.jmst.2023.09.054.
[23] Ayer Ö, Karakaya İ. Investigation of welding quality and internal elongation problem in aluminum extrusion. Journal of Manufacturing Processes 2023;106:254–64. https://doi.org/10.1016/j.jmapro.2023.10.001.
[24] Llorca-Schenk J, Rico-Juan JR, Sanchez-Lozano M. Designing porthole aluminium extrusion dies on the basis of eXplainable Artificial Intelligence. Expert Systems with Applications 2023;222:119808. https://doi.org/10.1016/j.eswa.2023.119808.
[25] Wang Y, Zang A, Mahmoodkhani Y, Wells M, Poole W, Parson N. The effect of bridge geometry on microstructure and texture evolution during porthole die extrusion of an Al–Mg–Si–Mn–Cr alloy. Metall Mater Trans A 2021;52:3503–16. https://doi.org/10.1007/s11661-021-06322-5.
[26] Wang Y, Zhao G, Sun L, Wang X, Wei D, Liu L. Effects of welding angle on microstructure and mechanical properties of longitudinal weld in 6063 aluminum alloy extrusion profiles. J Mater Res Technol 2022;17:756–73. https://doi.org/10.1016/j.jmrt.2022.01.054.
[27] Wang Y, Zhao G, Yu J, Wang X, Xu S. Optimization design of porthole die and study on microstructures and mechanical properties for an Al–Li alloy hollow profile. J Mater Res Technol 2024;29:400–15. https://doi.org/10.1016/j.jmrt.2024.01.138.
[28] Hölker R, Haase M, Ben Khalifa N, Tekkaya AE. Hot extrusion dies with conformal cooling channels produced by additive manufacturing. Materials Today: Proceedings 2015;2:4838–46. https://doi.org/10.1016/j.matpr.2015.10.028.
[29] Giarmas E, Tsakalos V, Tzimtzimis E, Kladovasilakis N, Kostavelis I, Tzovaras D, et al. Selective laser melting additive manufactured H13 tool steel for aluminum extrusion die component construction. Int J Adv Manuf Technol 2024;133:4385–400. https://doi.org/10.1007/s00170-024-14007-7.
[30] Ben Khalifa N, Isakovic J, Bohlen J. New concepts of extrusion dies to reduce the anisotropy of extruded profiles by means of additive manufacturing. CIRP Annals 2021;70:231–4. https://doi.org/10.1016/j.cirp.2021.04.006.
[31] Elsayed FR, Hort N, Salgado Ordorica MA, Kainer KU. Magnesium permanent mold castings optimization. Mater Sci Forum 2011;690:65–8. https://doi.org/10.4028/www.scientific.net/MSF.690.65.
[32] Nienaber M, Safieh N, Bohlen J, Ben Khalifa N. Influence of process parameters and die design on the microstructure and texture development of direct extruded magnesium flat products. In: Mocellin K, editor. Proceedings of the 14th international conference on the Technology of Plasticity - current trends in the Technology of Plasticity, ICTP 2023 - volume 1; 2024. p. 511–21. https://doi.org/10.1007/978-3-031-41023-9_52.
[33] Levanov A. Improvement of metal forming processes by means of useful effects of plastic friction. J Mater Process Technol 1997;72:314–6. https://doi.org/10.1016/S0924-0136(97)00191-X.
[34] Nienaber M, Kurz G, Letzig D, Kainer KU, Bohlen J. Effect of process temperature on the texture evolution and mechanical properties of rolled and extruded AZ31 flat products. Crystals 2022;12:1307. https://doi.org/10.3390/cryst12091307.
[35] Cano-Castillo G, Victoria-Hernández J, Bohlen J, Letzig D, Kainer KU. Effect of Ca and Nd on the microstructural development during dynamic and static recrystallization of indirectly extruded Mg–Zn based alloys. Mater Sci Eng A 2020;793:139527. https://doi.org/10.1016/j.msea.2020.139527.
[36] Jackson AG. Slip Systems. In: Jackson AG, editor. Handbook of crystallography, for Electron Microscopists and others. New York, NY: Springer New York; 1991. p. 83–8. https://doi.org/10.1007/978-1-4612-3052-6_7.
[37] Wu J, Jin L, Dong J, Wang F, Dong S. The texture and its optimization in magnesium alloy. Journal of Materials Science & Technology 2020;42:175–89. https://doi.org/10.1016/j.jmst.2019.10.010.
[38] Ha C, Bohlen J, Yi S, Zhou X, Brokmeier H-G, Schell N, et al. Influence of Nd or Ca addition on the dislocation activity and texture changes of Mg–Zn alloy sheets under uniaxial tensile loading. Mater Sci Eng A 2019;761:138053. https://doi.org/10.1016/j.msea.2019.138053.
[39] Agnew SR, Duygulu Ö. Plastic anisotropy and the role of non-basal slip in magnesium alloy AZ31B. International Journal of Plasticity 2005;21:1161–93. https://doi.org/10.1016/j.ijplas.2004.05.018.
[40] Victoria-Hernández J, Yi S, Klaumünzer D, Letzig D. Comparison of the mechanical properties and forming behavior of two texture-weakened Mg-sheet alloys produced by twin roll casting. Front. Mater. 2019;6:482603. https://doi.org/10.3389/fmats.2019.00288.
[41] Manik T, Marthinsen K, Zhang K, Aria AI, Holmedal B. Deformation texture evolution in flat profile AlMgSi extrusions: experiments, FEM, and crystal plasticity modeling. Front. Mater. 2021;8:1–12. https://doi.org/10.3389/fmats.2021.636379.
[42] Engler O, Yang P, Kong XW. On the formation of recrystallization textures in binary Al-1.3% Mn investigated by means of local texture analysis. Acta Mater 1996;44:3349–69. https://doi.org/10.1016/1359-6454(95)00416-5.
[43] Barrett CD, Imandoust A, Oppedal AL, Inal K, Tschopp MA, El Kadiri H. Effect of grain boundaries on texture formation during dynamic recrystallization of magnesium alloys. Acta Mater 2017;128:270–83. https://doi.org/10.1016/j.actamat.2017.01.063.
[44] Xu J, Zhao J, Jiang B, Liu W, Yang H, Li X, et al. Understanding the superior mechanical properties of Mg–3Al–Zn alloy sheets: role of multi-type unique textures. Int J Miner Metall Mater 2023;30:1104–12. https://doi.org/10.1007/s12613-023-2603-z.
[45] Bohlen J, Wendt J, Nienaber M, Kainer KU, Stutz L, Letzig D. Calcium and zirconium as texture modifiers during rolling and annealing of magnesium–zinc alloys. Mater Charact 2015;101:144–52. https://doi.org/10.1016/j.matchar.2015.02.002.
[46] Chen J, Poole WJ, Parson NC. The effect of through thickness texture variation on the anisotropic mechanical response of an extruded Al-Mn-Fe-Si alloy. Mater Sci Eng A 2018;730:24–35. https://doi.org/10.1016/j.msea.2018.05.105.